Environmental NMR: Solid-state Methods

Caroline M. Preston

Natural Resources Canada, Pacific Forestry Centre, Victoria, British Columbia, Canada

Solid-state NMR is widely used to characterize organic matter (OM), including litter inputs, peat, composts, and mineral soil, and to understand the fate of environmental contaminants. The combination of high-power decoupling, magic-angle spinning (MAS), and cross polarization (CP) to enhance sensitivity has greatly facilitated applications to ^{13}C, with lesser use of ^{15}N and ^{31}P. Focusing on ^{13}C, this article summarizes the development of the field and presents basic concepts of solid-state NMR, pulse sequences commonly used [direct polarization (DP), CP, dipolar dephasing (DD), and total sideband suppression (TOSS)], sample preparation and hydrofluoric acid pretreatment, general approaches to spectral acquisition and FID processing, removal of background signal, and data analysis including correction for spinning side bands (SSBs) and interpretation through a molecular mixing model of representative biopolymers. As CP NMR is inherently nonquantitative, and nuclei may be undectectable even with DP, techniques to improve quantitative reliability are discussed. More complex experiments can reveal spatially heterogeneous domains by generating subspectra of ^{13}C associated with protons with different relaxation times, and more recent developments allow spectral editing and two-dimensional (2-D) applications such as heteronuclear correlation (HETCOR). Applications of solid-state ^{15}N NMR are much more challenging, because of its low sensitivity and low natural abundance. Similarly, despite 100% natural abundance and high sensitivity, solid-state ^{31}P NMR is also limited by the small chemical shift range of phosphate minerals, and peak broadening and large higher order sidebands because of their close association with paramagnetics and large chemical shift anisotropy (CSA). However, studies with these nuclei can still provide much insight into OM cycling and the fate of fertilizers and contaminants in the environment.

Keywords: organic matter, solid-state NMR, CPMAS, ^{15}N NMR, ^{13}C NMR, ^{31}P NMR

How to cite this article:
eMagRes, 2014, Vol 3: 29–42. DOI 10.1002/9780470034590.emrstm1338

Introduction

Principles of NMR

The basis of NMR spectroscopy is that only certain atomic nuclei have a nuclear spin I, and thus a magnetic moment μ, which interacts with a static magnetic field. These nuclei include ^{1}H, ^{13}C, ^{15}N, and ^{31}P (Table 1[1]). In an external magnetic field B_0, which is represented as a vector in the z direction, such nuclei split into $2I+1$ energy levels, with the splitting proportional to the field strength B_0 and γ, a constant for each nucleus. Nuclei with $I = 1/2$, such as ^{1}H and ^{13}C, therefore, split into two populations. The very slight surplus of nuclei in the lower energy level, as determined by the Boltzmann equation, results at equilibrium in a macroscopic sample magnetization M_0 (Figure 1a). In fact, each nuclear spin is not statically aligned, but precessing around B_0 at the Larmor frequency ω, which corresponds to the energy gap ΔE:

$$\omega_0 = \gamma B_0 \qquad (1)$$

Rather than the laboratory (static) frame of reference, Figure 1 uses a reference frame rotating at the Larmor frequency, which simplifies the picture. In NMR, transitions between the energy levels are induced by a very brief pulse of a second oscillating magnetic field B_1, oriented perpendicular to B_0, which rotates the magnetization M_0 into the direction of the y-axis (Figure 1b). The angle of rotation is determined by the product of the strength and the duration of B_1; a 90° pulse rotates M_0 into the y-axis, a 180° to the z direction, and so on. The magnetization continues to precess around the y-axis, and the resulting periodic oscillation of the y-component of M_0 is picked up as an electrical signal induced in the coil surrounding the sample.

When a collection of nuclei is placed into the static magnetic field, the z-magnetization increases to M_0 exponentially according to the spin–lattice relaxation time (T_1). (T_1 and other relaxation times that we shall meet is the inverse of a rate constant.) Conversely, after a disturbance, such as a 90° pulse, the spins return to thermal equilibrium, as the excess spin energy is returned to the lattice at a rate similarly governed by T_1. At the same time, energy is redistributed among the spins, and the signal in the x–y plane is lost exponentially at the rate determined by T_2, the spin–spin relaxation time.

NMR is different from many other forms of spectroscopy. First, only nuclei with a magnetic moment are able to participate; for example, we may look at ^{13}C, with 1.1% natural abundance, but not the abundant isotope ^{12}C. Table 1 lists some nuclei of interest for organic matter (OM) studies; this article will focus on ^{13}C, with a brief introduction to ^{15}N and ^{31}P NMRs. Second, the energies involved in NMR are very low compared to infrared, or visible and ultra-visible light. This means that the equilibrium population differences are

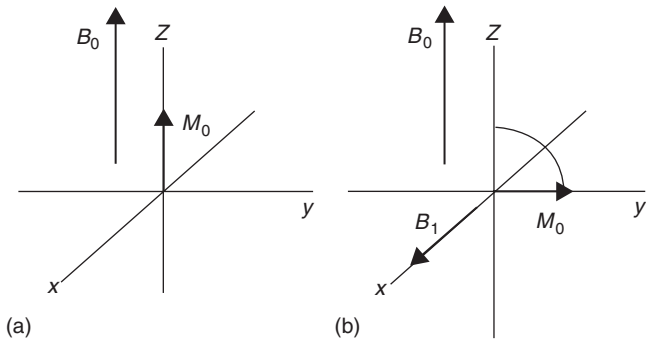

Figure 1. (a) Equilibrium magnetization M_0 in the rotating reference frame and (b) effect of a 90° pulse

Table 1. Properties of NMR nuclei used in solid-state environmental studies[1]

Nucleus	Spin	Abundance %	Frequency MHz @ 9.4 T	Sensitivity @ Nat. abun.	Chemical shift Reference
^{1}H	1/2	99.99	400.0	1.000	Me_4Si
^{13}C	1/2	1.07	100.6	1.7×10^{-4}	Me_4Si
^{15}N	−1/2	0.368	40.5	3.8×10^{-6}	$MeNO_2$
^{31}P	1/2	100	161.9	6.6×10^{-2}	85% H_3PO_4

extremely small, so that sensitivity is inherently limited. Third, the processes of spin energy transfer are much slower, which limits the rate of signal buildup and thus the repetition rate of NMR experiments. In higher energy spectroscopies, after a perturbation to put energy into the system, relaxation mainly occurs by re-emission of photons corresponding to the relevant energy gaps. The probability of this process basically increases as the third power of the energy (frequency)^2 and is completely inconsequential for NMR. To reach M_0, energy is transferred to (or acquired from) the lattice by several processes based largely on motional fluctuations corresponding to the frequency of the spin energy gaps. On the other hand, these slow processes allow much creative manipulation of magnetization in different types of experiments. Descriptions of basic NMR theory are widely available and basic summaries are found in several of the references cited herein.[3−5]

NMR Chemical Shifts

While the primary Larmor frequency of a nucleus is determined by its nuclear γ and the magnetic field strength, the local fields of nearby electrons act in opposition to shield the nuclei from B_0. This means that the signals are spread out across a range of chemical shifts (δ values), which generally increase with increasing electronegativity of carbon substituents and bond unsaturation, and are expressed in ppm from a reference frequency. For ^{1}H and ^{13}C, this is usually tetramethylsilane with δ of zero. The ppm scale is used as it is independent of the magnetic field strength permitting direct comparison of data collected on instruments at different fields. For example, with a 9.4 T magnet (400 MHz for ^{1}H), the ^{13}C Larmor frequency is 100.6 MHz, and 1 ppm would be 100.6 Hz.

Characteristic chemical shift ranges for ^{13}C with assignments typical for OM are listed in Table 2.[6,7] These are a general guide, and detailed studies should be consulted for specific compounds, including condensed tannins.[8,9] Alkyl C occurs at 0–50 ppm, with often distinct signals for CH_3 at 15 ppm and for long-chain CH_2 at 30 and 33 ppm. The sources of this alkyl C include waxes and cutin, which form the outer coating of leaves and fruit; the more complex biopolymer suberin, found in roots and bark; C4 of condensed tannins; and the sidechains of proteins. The region for alkyl C with O and N substitutions stretches from 50 to 112 ppm and is often subdivided into three regions: methoxyl C with a sharp peak at 57 ppm, *O*-alkyl C from 60 to 90 ppm, mainly dominated by carbohydrate C with single oxygen substitution, and 90–112 ppm for di-*O*-alkyl C, typical of the anomeric C-1 of carbohydrates. However, the *O*-alkyl region also includes the 3-carbon sidechain of lignin, C2 and C3 of condensed tannins, and primary and secondary alcohol esters of cutin. Aromatic C with C and H substitutions falls mainly within 112–140 ppm and phenolic C (aromatic with O-substitution) from 140 to 160 ppm. The aromatic and phenolic regions may be reported as a combined aryl region. For soil OM, aryl carbons are mainly associated with lignins, condensed and hydrolyzable tannins, and black carbon produced by fire (see Forest Ecology and Soils and Soil Organic Matter). Carboxyl/carbonyl C, including free carboxyls, amides, and esters, is at 160–185 ppm, with aldehyde and ketone signals found as far as 220 ppm. Proteins contribute to intensity in several regions: β, δ, and γ-CH_2 and CH_3 are found at 15–40 ppm; α-CH at 52–60 ppm, except glycine at 42 ppm; aromatic CH of phenylalanine and tyrosine at 130–155 ppm; O–C of tyrosine

Table 2. Main assignments for solid-state ^{13}C spectra referenced to tetramethylsilane at 0 ppm[6,7]

Chemical shift range (ppm)	Assignment
0–25	Methyl groups bound to C and CH_3 of acetate
25–45	Methylene groups in aliphatic rings and chains
45–60	Methoxyl groups, C6 of carbohydrates, and Cα of most amino acids
60–90	C-2–C-6 of carbohydrates, Cα of some amino acids, and higher alcohols
90–110	Anomeric C of carbohydrates, syringyl lingin C-2, C-6
110–140	Aromatic C–H, guaiacyl C-2, C-6, olefinic C
140–160	Aromatic COR or CNR groups
160–220	Carboxyl/carbonyl/amide groups

at 155 ppm; and C=O of amide linkages at 175 ppm.[9,7,10] With decomposition, signals from plant components decline and are increasingly replaced by those of the corresponding structures (lipids, carbohydrates, proteins, etc.) of microbial biomass and the 'molecularly uncharacterized components'.[11]

Development of Environmental Solid-state NMR

Early NMR spectrometers were based on electromagnets for field strengths up to 100 MHz for ^{1}H, and spectra were acquired through 'continuous-wave' processes as recounted in an interesting historical reflection.[12] The frequency of the oscillating magnetic field was varied slowly enough to avoid signal saturation, and the signals were detected when the magnetic field corresponded to an energy gap of the spin system; the whole process usually converted to movement of an ink-filled pen. Sometimes, cumbersome integrators summed the signals from multiple scans. Modern NMR is based on application of brief broadband pulses of radiofrequency energy covering the whole chemical shift range of interest. The decaying signal along the y-axis is called the free induction decay (FID), the sum of the time-domain signals from all frequencies. Fast Fourier transformation (FFT) from the time-to-frequency domain results in a spectrum in which, ideally, the intensity at each chemical shift is proportional to the number of corresponding nuclei.

For many decades, applications of NMR in organic chemistry were limited to soluble samples with regular structures, whereas attempts to obtain information from solids faced seemingly insurmountable obstacles.[13] First, in many molecules, the electron distribution around a nucleus is anisotropic, so that the chemical shift depends on the orientation of each molecule to B_0. In liquids, this chemical shift anisotropy (CSA) averages to zero because of molecular tumbling and a sharp line is observed (extreme-narrowing limit). In solids, however, CSA results in very broad asymmetric signals. Second, the interactions among nuclei result in splitting of energy levels and multiple lines. In molecules rotating freely in solution, these interactions similarly average to zero, and the resulting intramolecular (e.g., ^{1}H–^{1}H and ^{13}C–^{1}H) coupling patterns can be directly related to the molecular structure. However, in solids, where spins are held rigidly with respect to each other, dipolar interactions result in significant broadening. That is, one spin 'sees' each neighbor's spin as a perturbation of B_0, resulting in a different chemical shift. Finally, ^{13}C typically has long relaxation times for soil and geochemical samples, of the order of seconds to minutes, as well as low natural sensitivity, because of both low γ and low natural abundance (Table 1).

Some three decades later, it is hard to imagine the excitement generated by the initial demonstration of a new combination of techniques to generate chemically meaningful solid-state ^{13}C NMR spectra of complex organic samples,[14] and quickly applied to fossil fuels,[5] humic fractions,[15] peat,[16] and mineral soils.[17] Broadening due to dipolar coupling and CSA was overcome by high-power decoupling and magic-angle spinning (MAS), respectively, and sensitivity was enhanced by cross polarization (CP), which counteracts both the long relaxation times of ^{13}C and its inherently low sensitivity. Applications to OM developed rapidly,[6,18,19] and recent years have seen continuing increases in magnetic field strength, spinning speed, and the complexity of pulse sequences.

Basic Techniques for Environmental Solid-state NMR

High-power Decoupling

Because of the low natural abundance of both ^{13}C and ^{15}N, homonuclear coupling is inconsequential compared to heteronuclear interactions with ^{1}H. The basis of heteronuclear decoupling is the application of another continuous B_2 field over the whole range of ^{1}H frequencies. This perturbs the ^{1}H spins by inducing fast transitions, so that the ^{13}C or ^{15}N nuclei 'see' only an average interaction. Broadband ^{1}H decoupling has long been used for solution ^{13}C NMR, but solids require much higher power because of the greater spread of ^{1}H chemical shifts, and care must be taken to avoid overheating or equipment damage by excessive acquisition times, or too-short relaxation delays. The pulse sequences shown later depict an invariant ^{1}H power level during decoupling, as was the case for many older instruments, including some still functioning. However, more complex decoupling schemes use reduced power while improving sensitivity and resolution,[20] the most widely used being two-pulse phase-modulated (TPPM) decoupling.[21]

Magic-angle Spinning (MAS)

MAS was independently reported in 1959 for removal of ^{23}Na homonuclear dipolar broadening in a crystal of NaCl[22] and of ^{19}F interactions in CaF_2 and teflon.[23] The dipolar interactions are proportional to $3\cos^2\beta - 1$, where β is the angle between the static magnetic field B_0 and the internuclear vector. At $\beta = 54.7^{\circ}$, the result is zero, so that spinning at the magic angle effectively cancels dipolar interactions, substituting for the motional averaging, which occurs in liquids. To be effective, the spinning rate has to be at least as high as the width of the broadening caused by the interactions, so that MAS does not in fact compensate for the much larger ^{1}H–^{13}C or ^{1}H–^{15}N dipolar interactions, which are mainly dealt with by high-power decoupling; however, in the same way, MAS effectively counteracts the broadening due to CSA. If the spinning rate is not high enough, however, the peak breaks up into a series of spinning side bands (SSBs) on each side of the central peak at multiples of the spinning speed. Thus, if the MAS rate is 5000 Hz, and the Larmor frequency for ^{13}C is 25 MHz, the SSB appear at intervals of 200 ppm and at low intensity compared to the central peak. If the Larmor frequency is 100 MHz, the SSBs are now both larger and only 50 ppm from the central peak, enough to cause serious interference.[24] The intensity of SSB is proportional to the CSA, so that they generally increase with increasing chemical shift; i.e., with increasing O and N substitutions and bond unsaturation, and thus are usually inconsequential for alkyl C with its more symmetric distribution of electron bond density.

Single-pulse Acquisition

Figure 2(a) shows the pulse program for a simple acquisition, usually referred to as direct polarization (DP) and also described

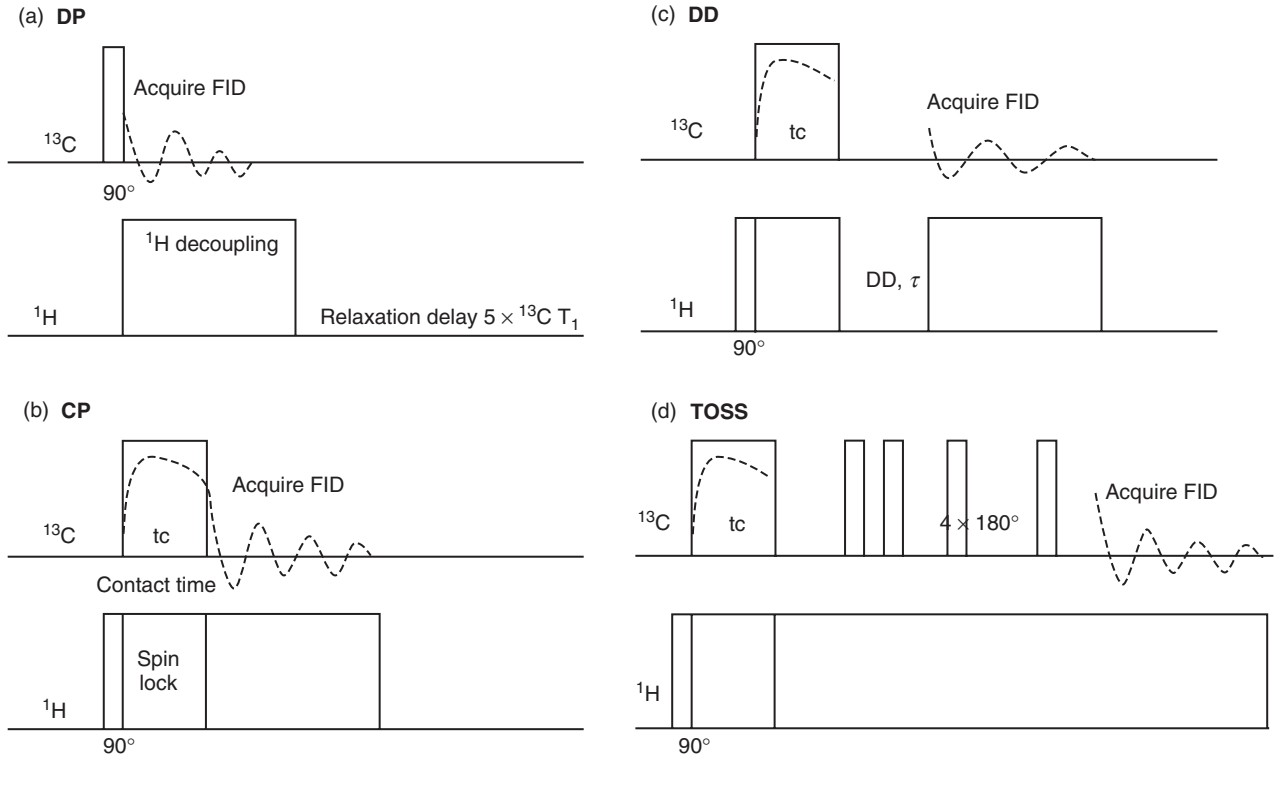

Figure 2. Pulse sequences for acquisition by (a) direct polarization (DP), (b) cross polarization (CP), (c) dipolar dephasing (DD), and (d) total sideband suppression (TOSS)

as single-pulse excitation (SPE) or Bloch decay (BD). A 90° pulse (typically, <5 μs) rotates the ^{13}C magnetization into the y-axis, and immediately following, ^{1}H decoupling is applied along the y-axis during FID acquisition, after which the decoupler is turned off to allow the spins to return to the equilibrium. This duration is determined by the ^{13}C T_1, with full relaxation requiring five times the T_1 value. For most OM samples, the FID decays rapidly, within 10–20 ms, and there is no point in recording for much longer than its length. Once the FID has decayed to essentially noise level, longer acquisition produces little additional information for the broad signals of OM samples, while unnecessarily increasing the duration of most high-power decoupling. For all acquisitions, the FID should be examined to verify that the acquisition time is appropriate, and to check for low signal that indicates a malfunction, or for artifacts such as spikes due to excessive sample conductivity, as can happen with soot, for example. Delay times required for complete relaxation are often 100 s and/or longer.[25] A background-corrected DP spectrum of a mineral soil with 29 mg C g^{-1} (Figure 3b[26]) shows the poor signal-to-noise ratio (S/N) usually obtained with a limited number of scans. DP spectra of OM usually have broader peaks and more rolling baselines as a result of better detection of carbon close to paramagnetics such as iron. This can include some very broad lines with short ^{13}C T_2; the resulting FID is characterized by a short initial spike of intensity, which causes baseline distortion (see section titled 'Processing the FID').

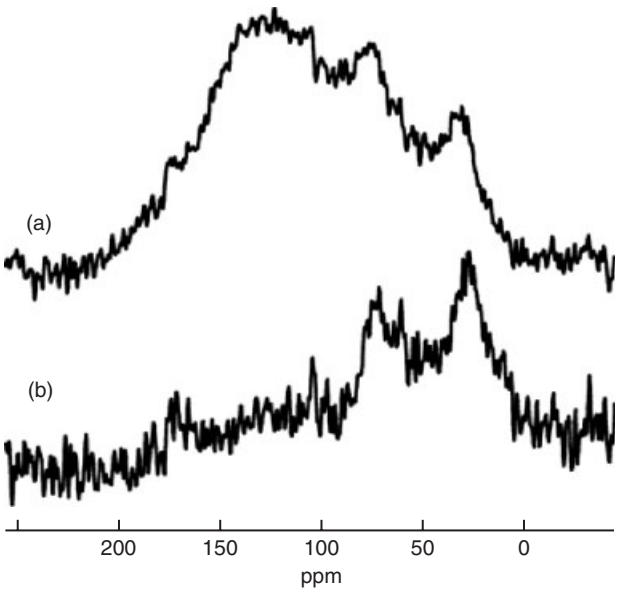

Figure 3. Solid-state ^{13}C direct polarization MAS spectra of (a) A-horizon mineral soil with 29 mg C g^{-1} and (b) after background correction. (Reproduced from Ref. 26, with the permission of Natural Resources Canada, 2002)

CP and CP with TOSS

In environmental samples, protons are often much more abundant than ^{13}C nuclei. For ^{1}H, the γ is four times higher and

their T_1 values in OM samples are typically <2 s. By transferring magnetization from ^{1}H to ^{13}C before acquisition, CP can enhance ^{13}C signal intensity to a theoretical maximum of fourfold[27] and reduce the relaxation delay to that determined by the T_1 of protons. For magnetization to be transferred between spins of different γ, their ΔE must be equal; i.e., the Hartmann–Hahn condition must be fulfilled:[28]

$$\Delta E_H = \Delta E_C = \gamma_H B_{1H} = \gamma_C B_{1C} \quad (2)$$

This is accomplished by rotating both spins into the y-axis, and applying simultaneous B_1 fields adjusted to satisfy equation (2). During this spin-locked condition, both spins precess around z with the same frequency, and magnetization is transferred from ^{1}H to ^{13}C spins during the contact time (tc). At the end of tc, which is typically 0.5–1.5 ms for OM, the ^{13}C B_1 field is turned off and the ^{13}C signal acquired with ^{1}H decoupling, as for DP (Figure 2b).

More detailed theory and the equations describing the transfer of magnetization are available elsewhere,[25,29,30] but basically, the changes in the ^{13}C magnetization are controlled by two competing mechanisms. As shown schematically in Figure 2(b), this generally results in a fairly rapid increase in ^{13}C intensity, followed by a slower decline. The former is controlled by the CP transfer time constant T_{CH}, but at the same time, ^{1}H magnetization is lost exponentially during the spin-locked state. The time constant for this is $T_{1\rho H}$, the spin–lattice relaxation time in the rotating frame. Considering only the effect of distance from protons, T_{CH} is the shortest for CH_2 and CH_3, slower for CH, and the slowest for nonprotonated ^{13}C, especially for those remote from protons, as in highly condensed aromatic structures or carbonate.[19,29,31] However, CP is also weakened by molecular motions, which can occur even in the solid state and also have the effect of decreasing dipolar interactions.[32] Rotation of CH_3 groups and movement of CH_2 in long chains result in less-efficient CP for carbons in methyl and methoxyl groups, and long-chain hydrocarbons. Because of the variations in T_{CH}, and internal motion, the resulting CP enhancements are variable, resulting in a lack of quantitative reliability in the relative areas of the spectrum. For carbons remote from protons, CP can be very weak, as the pool of ^{1}H magnetization available for transfer is largely lost through $T_{1\rho H}$ before it can be transferred. As discussed in the section titled 'Using more Complex Pulse Sequences', the CP efficiency is also affected by paramagnetics such as Fe^{3+}, which can drastically shorten $T_{1\rho H}$.

For most OM samples, the intensity enhancement due to CP is closer to 2 than the theoretical maximum of 4.[4] For a set of fresh and decomposed foliar litter samples, CP/DP ratios were determined by the comparison of CP and DP intensities for spectra acquired with the same number of scans.[33] Mean CP/DP ratios were alkyl = 1.9, methoxyl = 2.0, *O*-alkyl = 2.3, di-*O*-alkyl = 2.0, aromatic = 1.5, phenolic = 1.3, carboxyl = 1.4, and 1.8 for overall intensity. Enhancements were lowest for carboxyl, phenolic, and aromatic C, and highest for *O*-alkyl C, as expected from their relative ease of CP.[34] The intermediate value for alkyl C may reflect variable CP efficiency as a result of the relative proportions of rigid and mobile C. The CP advantage thus results from the combination of intensity enhancement and greatly reduced relaxation delays. Figure 4(a)[19] shows the good S/N easily obtained for a sample with 56% C.

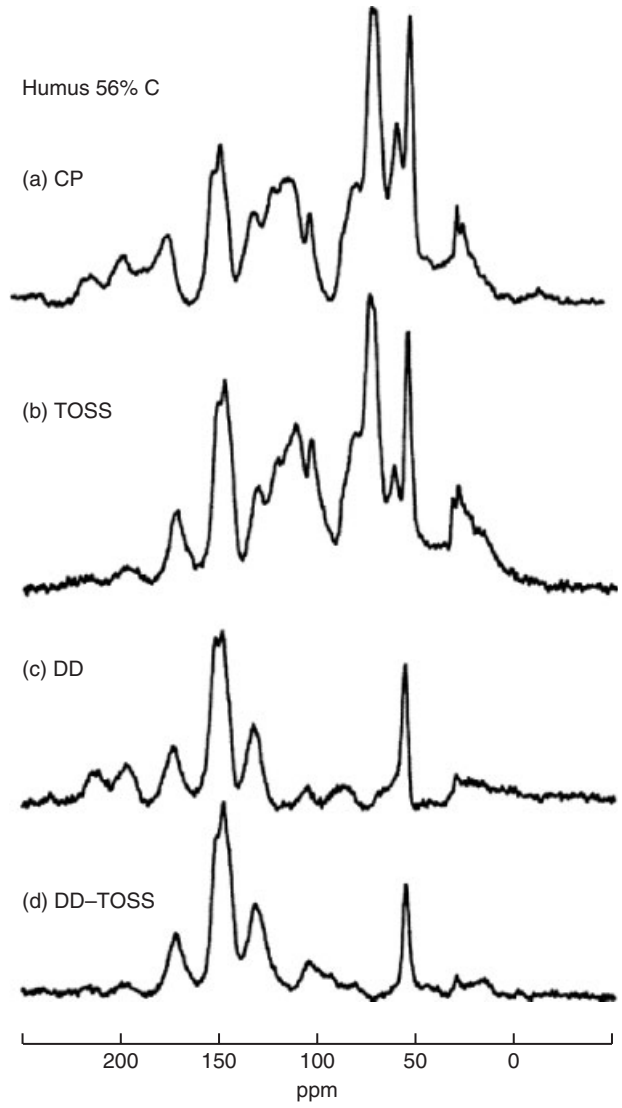

Figure 4. Solid-state ^{13}C MAS spectra of forest floor from Vancouver Island (560 mg C g^{-1}) for acquisition with (a) CP, (b) TOSS, (c) DD, and (d) DD–TOSS. (Reproduced with permission[19])

With increasing magnetic field strengths, higher spinning speeds are required to overcome SSBs, so that the broad H–H matching profile breaks up into a series of narrow bands separated by the spinning speed. To compensate for this, the fixed ^{1}H power level during CP is replaced with a ramped amplitude (RAMP) CP ^{1}H power profile.[4,35,36] RAMP-CP is now in wide use, although like TPPM decoupling, may not be available on older instruments, and also requires additional steps in the experimental setup. Especially at higher spinning rates (ca >6000 Hz), RAMP-CP should be set up on the −1 sideband rather than the center band, and after initial setup on a standard such as glycine, it should be optimized, as far as possible, on a representative OM sample. A recent study presents a very detailed analysis of the effects of ramp size

and spinning speed on CP intensity for two humic acids and recommendations for OM.[37]

If it is not possible to remove or minimize SSBs by fast spinning, they can be suppressed using the TOSS variant of CP, as shown for the same forest floor sample in Figure 4(b). TOSS incorporates a series of four ^{13}C 180° pulses with variable spacing between the contact time and signal acquisition, during which time the decoupler remains on (Figure 2d).[38] Calculation of these delay times is based on the spinning speed, as reviewed in more detail elsewhere,[39] but usually this is done automatically once the MAS rate is entered. During this time, some intensity is lost because of T_2 relaxation of ^{13}C, so that T_2 variation could result in selective intensity loss.[40] For a wide range of fossil fuel samples, aromaticity was only slightly lower for TOSS than for normal CP, but one peat sample showed greater loss of alkyl C.[41]

Intensity loss has been reported with TOSS,[20,39,42] but published quantitative evaluations of TOSS-induced intensity losses for OM have not. In additional unpublished work on the foliar litters used in a previous study,[33] it was observed that the overall TOSS intensity was 63% of the corresponding CP spectra for ^{13}C at 75.47 MHz with spinning at 4300 Hz. The differentials [(TOSS-CP)/CP] were positive for alkyl (4.2%) and *O*- and di-*O*-alkyl C (6.8%) and negative for methoxyl (−12%), aryl (−11%), and carboxyl (−16%) C. However, TOSS was less successful for highly aromatic char samples, as the resulting spectra are prone to artifacts, and difficult to phase, and comparison of intensity distributions is further complicated by the difficulty of making the SSB corrections for the CP spectra.

Dipolar Dephasing (DD) and DD–TOSS

With dipolar dephasing (DD), which is a variant of CP,[43] a slight delay without decoupling is inserted between T_{CH} and signal acquisition (Figure 2c). During this delay, signal is rapidly lost from carbons that have the strongest dipolar interactions with protons; i.e., the same groups with the shortest T_{CH}. Signal is lost more slowly for carbons with weak dipolar coupling, thus with no attached protons, or weakened because of internal motions. Like CP, DD is also slower at higher spinning speeds. A dephasing time around 45–50 μs typically results in complete loss of carbon in rigid structures with attached protons, so that the resulting DD spectrum retains carbon without attached protons, and those with some motional freedom. The dephasing time should be adjusted for complete loss of the *O*-alkyl C signal. A series of similar samples should be analyzed using similar dephasing times. For the DD–TOSS combination, the delays are similarly calculated based on the MAS speed. Because DD spectra are dominated by carbons with greater CSA, the SSBs can be very prominent as shown in Figure 4(c). Especially, if the goal is qualitative structural information, the combination of DD with TOSS provides an unobstructed view of peak shapes and positions (Figure 4d).

The DD–TOSS forest floor spectrum (Figure 4d) is dominated by carboxyl and aryl C without attached hydrogen and also has peaks for methoxyl C at 57 ppm and long-chain alkyl C at 30 ppm. A small peak or shoulder may also be observed at 15 ppm for terminal methyl C. The CH_2 peak is often observed to have two maxima, at 30 and 33 ppm, with the latter lost rapidly under DD, whereas the 30 ppm peak represents long-chain CH_2 with greater mobility.[44–46] The 50–60 ppm region, often attributed to methoxyl C in the standard division of spectra into chemical shift regions, is also the region where C–N from amino acids resonates. During DD, the broad C–N intensity is rapidly lost, leaving the sharper peak of methoxyl at 57 ppm, a characteristic feature of lignin.[9,10,47] The DD spectra also help clarify the relative importance of lignin and condensed tannins. In the di-*O*-alkyl region, condensed tannins have a broad peak at 106 ppm (C10 and C8 in C4 → C8 linkages), in a region usually otherwise lacking intensity in the DD spectrum. In the phenolic region, condensed tannins also have characteristic sharp peaks of 144 and 154 ppm, compared to the broader signal of lignin at 147–153 ppm.[9] The DD–TOSS spectrum is also useful to ascertain whether intensity beyond around 190 ppm in the CP spectrum is due to carbonyl C, or to SSBs, thus providing information to guide SSB correction.

While much qualitative information can be obtained using the basic DD pulse sequence, in addition to dipolar interactions, the intensities are also strongly modulated by effects due to CSA, MAS, and static field inhomogeneity, resulting in faster intensity loss, nonexponential decays, and even oscillations between negative and positive signals.[32,48,49] These artifacts are partially eliminated by a pulse sequence with a 180° refocusing pulse on both ^{1}H and ^{13}C channels.[32,50] Further isolation of dipolar interactions is obtained by using only the ^{13}C refocusing pulse, but with the interval between T_{CH} and FID acquisitions corresponding to two full MAS rotations, or multiples thereof,[51,52] although more intensity is lost because of ^{13}C T_2 relaxation during the longer delay times required by rotor synchronization.

Because carbons lose intensity at different rates during dephasing, a series of spectra run with different dephasing times can be used to determine the contribution of each peak to the normal CP at zero dephasing time.[32,47] However, time sequences using the rotor-synchronized ^{13}C refocusing pulse yield DD rate constants ($1/T_{2DD}$), which can provide valid information on distance to nearest protons, proportion of nonprotonated aromatics, and molecular mobility.[52] Using intervals up to eight rotor periods (1600 μs) and dephasing times up to 750 μs, the same authors[52] used linear combinations of CP and DD spectra to generate subspectra of three classes of OM carbon: nonprotonated, methyl, and nonmethyl protonated.

Acquiring and Processing Spectra

Sample Preparation and Packing

For many samples, the only preparation required is drying and grinding into a fine powder. Samples should be stored to minimize moisture sorption, or redried before use, with extra care for hygroscopic samples such as isolated OM extracts.[25,53,54] Changes in relaxation times and increased mobility due to sorption of water result in reduced sensitivity and distorted intensity distribution. Coarse or uneven particle sizes make it difficult to achieve a high spinning speed, especially with larger rotors, and the sample must be carefully packed down

in layers. With the larger 7 mm rotors, a little glass wool on the top may prevent particles from attaching themselves to the cap and causing imbalance. Especially, in larger rotors with manual MAS controls, speed is increased slowly to allow the particles to arrange themselves, which typically occurs around 1000 Hz. The centrifugal forces leave an empty cone in the center with particles packed toward the bottom and sides.[55] The consequences of this for signal strength are discussed later. Dilution with Al_2O_3 may work for samples unwilling to spin, and is also essential for highly conductive samples, such as soot and some charcoals.

Sample Pretreatment with Hydrofluoric Acid (HF)

Even with CP, it can be difficult or impossible to obtain spectra with high S/N for mineral soil samples because of their low total carbon and the impacts of paramagnetic species such as Fe^{3+} and Cu^{2+}. Interactions with unpaired electrons drastically reduce $T_{1\rho H}$, thus causing rapid loss of ^{1}H magnetization and hindering its transfer to ^{13}C.[34,56–59] Even for DP spectra, broadening of ^{13}C signals due to proximity of paramagnetic ions may also render them invisible. Ferromagnetic domains also degrade signal quality by broadening the ^{13}C signals due to distortions of the local field.[60] Size or density fractionation of mineral soils often yields silt or clay fractions with higher C content, which still may require pretreatment with hydrofluoric acid (HF). HF reacts with silica to form soluble fluoride complexes, dissolving the mineral matrix and magnetic impurities, and usually, increasing the carbon concentration of the remaining OM. Samples rich in carbonates should be pretreated with hydrochloric acid (HCl) to increase the relative concentration of organic C.

Mineral soil samples are generally treated with 5–10% v/v HF by shaking or stirring several times at room temperature,[61] followed by washing with water. HF/HCl mixtures are also used, especially if carbonates are present,[57,60,62–64] and removal of ferromagnetic particles may be aided by shaking with a magnetic stir bar.[65] HF is extremely hazardous and safety procedures must be followed;[63] HF-treated samples may also damage analytical instruments, as similarly found by the author.[61,66]

Pretreatment of samples with acids may result in OM losses, and for some soils, such as acidic forest subsoils, carbon losses can be quite high sometimes with little enhancement of organic C concentration.[67,68] However, quality of spectra generally still improves because of the removal of paramagnetic minerals. This can be especially important for *O*-alkyl C of carbohydrates because of their close interactions with paramagnetic ions such as Fe^{3+}, Mn^{2+}, Cu^{2+}, and VO^{2+}.[56,69–71] Of course, a primary concern is whether the remaining carbon is representative of the original total carbon, but these changes are difficult to quantify for low-C samples with poor or nonexistent pretreatment spectra. Most studies indicate only small effects of HF treatment, with some indications that carbohydrates are more likely to be lost.[60,61,64,66,67,72,73] Recently, HF treatment has been utilized as another approach to probe the nature of mineral-associated OM and mechanisms of C stabilization.[58,74]

Instrument Setup

Choice of acquisition conditions includes consideration of magnetic field, rotor size, and available MAS rate. Small rotors hold less amount of sample, and due to the smaller coil, exhibit higher mass sensitivity, larger excitation bandwidth, and spinning may be easier to achieve, albeit with a reduced sample volume. They are also often the only choice at high spinning speeds (i.e., ca >5000 Hz). The combination of higher magnetic field and low spin rate means more interference from SSBs, and may necessitate more use of TOSS and DD–TOSS. Each instrument and probe has its own characteristics, which need to be optimized. For most probes, the magic-angle position of the rotor is quite stable and need only be checked occasionally, or after some modification such as coil replacement. This is conveniently done by maximizing the number and intensity of sidebands on the ^{79}Br signal of KBr.[20,39] The Larmor frequency of this quadrupolar nucleus is very close to that of ^{13}C (50.12 MHz compared to ^{13}C at 50.306 MHz), so only a quick probe tuning is necessary.

As for ^{1}H, chemical shifts of ^{13}C are reported with respect to tetramethylsilane at 0 ppm. The COOH signal of glycine at 176.49 ppm[73] is often used as an external chemical shift reference, to establish the CP match, optimize shimming and measure the ^{1}H 90° pulse length. This is done indirectly by looking for the null of the CP ^{13}C signal at the ^{1}H 180° pulse. The ^{13}C 90° pulse length is also checked using DP acquisition, and both should be <5 μs. Measuring the actual CP enhancement of this signal is also a good practice. Using previously reported optimum acquisition parameters,[34] the author obtained similar CP/DP ratios of 3.3 for C1 and 3.5 for C2 (32 ppm) of glycine, and 3.5 (overall) for cellulose. Especially at higher spinning speeds, it is important to establish CP at the spinning rate to be used, and also on an actual sample, rather than glycine, but this is not always practical. For ^{13}C spectra of charcoal at 75 MHz and MAS >7000 Hz on a system without RAMP, good results were obtained by setting up CP on the −1 sideband,[4] using ^{13}C1-enriched glycine to improve the S/N. A mixture of ^{13}C1- and ^{13}C2-enriched glycine provides an additional peak for testing spectrometer performance. The chemical shift reference setting should also be checked occasionally using a sample of adamantane (42 ppm). The narrow linewidth of this signal also makes it useful for optimizing shimming, even if many OM samples have much broader peaks.

Background Signal

Especially with older instruments, a broad background signal may be produced mainly from probe ringdown, resulting from very broad lines with short-lived FIDs, general instrument noise, and C-containing components in the probe. The latter are mainly produced from components outside the coil volume, and in particular, the signal from caps made of Kel-F (poly(chlorotrifluoroethylene)) is negligible for CP spectra.[33,75] Background signal is not usually a problem for CP spectra of samples high in C, but of more consequence for low carbon and DP spectra (Figure 3). Background was equivalent to 1 mg of observable C (C_{obs}) for CP acquisition,[75] but for DP, amounted to 69[75] and 100 mg,[33] comparable to the C_{obs} in the sample. To

correct for this, the FID is acquired of an empty rotor under the same conditions as the sample. The rotor may be filled with Al_2O_3 if required for spinning stability. It is useful to record the background FID at a series of increasing number of scans, and such a series may be applied to many subsequent acquisitions. The background FID is subtracted from the sample FID, with scaling if necessary to match the number of scans. If FID subtraction does not work (e.g., FIDs were acquired with different sweep widths and computer glitches), the final phased, baseline-corrected spectra can be subtracted, although this is subject to more operator influence.

Another approach is to use a background generated by the actual sample.[76] Background signals that appear in the spectrum mostly arise from probe components outside the coil (usually, Kel-F or Teflon), which thus effectively experience a much weaker pulse than the sample. The sample signal increases with pulse length as a cosine function, whereas the background only increases linearly. For CP spectra, at a ^{1}H pulse length corresponding to 180° for the sample (a null signal), the background signal should be twice that of its value at a 90° pulse. Therefore, subtracting one-half the 180° signal from the 90° signal should leave a background-free signal. The 180° spectrum also provides a sensitive check of the ^{1}H 90° pulse for the actual sample, as any strong peak produces a residual signal in the background, and often, the pulse length can be adjusted after observing a few acquisitions. Similar to the empty-rotor background, this background may be used for similar samples and acquisition conditions. This method can also be used for DP spectra with 180° and 90° carbon pulses. An alternative approach suggested for DP spectra is a pulse sequence incorporating ^{19}F–^{13}C dipolar dephasing.[75]

Processing the FID

For most OM spectra, before Fourier transformation (FT), the FID is modified to enhance S/N. The simplest method is to apply a decaying exponential, which emphasizes the early part of the signal, an operation corresponding to 30–100 Hz linebroadening (LB). The amount of LB should be varied to get the best result, as excessive LB results in loss of detail and even baseline distortion. Spectra of OM, especially those with low C, or DP spectra, may be distorted by low-frequency artifacts, including probe ringdown, which appear as a spike at the beginning of the FID. Sometimes, the resulting spectrum can be improved by removing the first two or four points by setting their value to zero, or left-shifting the FID. Soil OM spectra usually need more aggressive phasing than usual, as well as baseline correction; examples are shown elsewhere.[19,63]

Some Approaches to Spectral Analysis

Aside from questions of quantitative reliability, OM spectra may need more care in integration. Integrals may be distorted by noise and curved or rising baselines, and if values seem unreliable, integral areas should be measured by hand. Copying, cutting, and weighing of spectra may occasionally be useful to obtain relative areas.[9,42] Measurement of relative areas is also complicated by peak overlap. For example, the broad wings of aryl C may extend into carboxyl and *O*-alkyl regions for charcoal samples, so that some sketching in of shoulders ('manual deconvolution') is more useful than applying the usual chemical-shift boundaries. It may be necessary to correct for the SSB intensity of the aromatic, phenolic, and carboxyl regions, and this is done by assuming equal intensity of the upfield and downfield SSB peaks. For many spectra, SSB can be weak and difficult to measure; for a large series of litter spectra, mean percent SSBs from the CP spectra were then used to correct both CP and DP intensities.[33] Deconvolution could probably be applied much more widely to ^{13}C OM spectra, especially for poorly decomposed samples, such as litter and organic horizons, which have a good peak definition.[19,72,77,78]

A molecular mixing model (MMM) has been developed to analyze NMR spectra as a mixture of five biochemical components: carbohydrate, protein, lignin, lipid, and black carbon and an extra pure carbonyl component to account for uronic acids and oxidation of other components.[79] The MMM uses the distribution of signal intensity in seven chemical-shift regions and the elemental composition of the representative biopolymers, and applications include soil[80] and peat.[81] The model is an extremely useful tool for understanding OM formation and decomposition over a wide range of situations. However, it is important to remember that the results are subject to the usual caveats regarding quantitative reliability of the spectra. Furthermore, as noted previously, with decomposition, the proportion of C that can be identified from chemical analysis decreases,[11] so that intensity identified as, e.g., carbohydrate or protein, might yield only a small proportion of that C as monosaccharides or amino acids upon hydrolysis.

Some suggestions could be made for further development. Plant litters can be very high in condensed tannins,[9,33] of which at least the more soluble portion is rapidly lost. Studies with a focus on litter decomposition could benefit by adding a CT component to the model. Most NMR data analyses, including the MMM or widely used principal component analysis (PCA), are also still based on the distribution of intensity into chemical-shift slabs. It would be interesting to see the results of an MMM using linear combinations of actual spectra of the representative biopolymers, or PCA with the NMR spectra as inputs, so that the loadings for each component come out as subspectra, as used for solution spectra in metabolomics.[82] As most solid-state OM ^{13}C NMR spectra can be well described with 1024 or even 516 data points, these analyses are quite feasible, as already demonstrated for peat in 1989.[83]

Toward Quantitative Reliability

The benefits of CP acquisition remain essential for most routine environmental applications of solid-state NMR, but its quantitative reliability has always been an issue.[3,25,34,57,73,78,84] In an ideal world, a DP spectrum would detect 100% of the C (see 'spin counting' discussion later in this section) and quantitatively represent the distribution of carbon structures. As long as the ^{13}C relaxation delay is long enough, this is the case for simple organic molecules and even for more complex substrates such as wood, which are low in paramagnetic

species.[34,85] In practice, however, the long acquisition times, problematic baseline distortions, and poor S/N of DP spectra generally make them impractical for routine application, even with carbon-rich samples. For OM samples, C_{obs} may still be quite low because of excessive broadening of C close to paramagnetic centers. For pyrogenic C (charcoal), however, with low CP efficiency and high total C, DP may sometimes be the better option.

Moreover, in an ideal world, CP enhancement would be the same for all carbon, even if not the theoretical maximum. However, as discussed previously in the section titled 'Background Signal', CP intensities are determined by T_{CH} and $T_{1\rho H}$ both of which vary with C structure and proximity to paramagnetic centers, and their opposing effects during the contact time tc. Ideally, if $T_{CH} \ll tc \ll T_{1\rho H}$, CP is complete before much ^{1}H polarization is lost because of $T_{1\rho H}$ relaxation. This situation is only met for a small proportion of sample, i.e., rigid CH_2 and CH_3 free from paramagnetic influence. However, contact times around 1 ms generally have been found to give the best overall CP intensities for OM.[25,34,69] Longer contact times may be used to enhance the aryl intensity of pyrogenic C, but there is usually little benefit beyond 2–3 ms, as the losses due to $T_{1\rho H}$ increasingly predominate.

Spin counting has long been used to determine C_{obs} for both CP and DP acquisitions, the assumption being that 100% observability corresponds to quantitative intensity distribution. For spin counting, the total signal due to the sample is compared with that of a standard such as glycine or cellulose often run separately.[34,57,65,85,86] Spin counting is also possible with internal standards mixed in with the sample, but these introduce other complexities, including overlap with sample peaks or alterations in the relaxation properties of the standard because of interactions with the sample.[87] Sensitivity also varies with position within the rotor,[34,55,88] and even well-mixed materials may migrate to different parts of the rotor with spinning. Inserts have been used to center a capillary of standard along the axis of a large rotor[72] or to place samples at different points along the rotor axis;[34] presumably, the latter could be used to position a layer of standard separated from the sample. If sample recovery is not a requirement, a simpler approach might be to first weigh in a small amount of standard, such as ^{13}C-enriched glycine or silicone rubber, and then pack the sample on top. This avoids the complexities of inserts, and a calibration could be developed to compensate for the lower response at the end of the rotor. The effect of sample position was determined rather simply by measuring signal intensity after successive additions of adamantane and measuring the depth occupied by the sample.[55]

Several approaches have been devised to overcome or compensate for the variability in CP intensities. If CP/DP enhancements are measured on a representative sample, correction factors can be applied to a series of similar samples.[89] For higher field instruments, the combination of RAMP and high-speed spinning may yield CP intensity distributions very close to those obtained by BD acquisition.[4,90] However, this may not overcome the very limited potential of CP for highly condensed aromatic samples; also such tests are usually carried out on relatively clean and high-C samples. As such, the extension of such comparisons; also to low-C samples requires further examination.

The most reliable (and time-consuming) approach is to run a series of spectra with variable contact times (VCT) and fit the resultant intensities to the equation describing the CP dynamics.[3,4,25,77,87] This yields the theoretical maximum CP intensity at zero tc if T_{CH} were infinitely short and $T_{1\rho H}$ infinitely long. A simplified version can be used to extrapolate intensities back to $tc = 0$ or to determine $T_{1\rho H}$ using only the decaying part of the curve mainly controlled by $T_{1\rho H}$ relaxation.[34,69,91] If not practical for routine application, such VCT data provide insights into the factors affecting CP for specific C structures or environments, guidance for choosing the best tc for routine CP acquisition, or correction factors applicable to a series of related samples.[77]

Using More Complex Pulse Sequences

^{1}H Relaxation- and T_{CH}-based Spectral Editing

To this point, relaxation processes have been considered as simple exponentials characterized by a single rate constant, as would be the case for most pure chemicals. However, many OM samples exhibit spatial heterogeneity at the nanometer scale with separation into domains that present barriers to spin diffusion, resulting in two- or even three-component relaxation behavior.[84] Differences in proton relaxation rates can be used to separate the subspectra of C in domains on the order of 30–100 nm for T_{1H} and around 2–30 nm for $T_{1\rho H}$. Proton spin relaxation editing (PSRE) separates C in domains with different proton T_1 values.[92,93] If the ^{1}H magnetization is initially inverted by a 180° pulse and a CP spectrum taken after different delay intervals, the ^{13}C signal recovers from negative to positive intensity. In a structurally homogeneous solid with strong dipolar $^{1}H-^{1}H$ coupling, spin diffusion leads to an average value for T_{1H} and signal recovery follows a simple exponential. If ^{1}H relaxation is a sum of two components, at a certain delay interval, the signal from the ^{13}C associated with slowly relaxing protons is passing through the null point, whereas that of the fast-relaxing component has already almost recovered to full intensity, so that the slow component is missing from the resulting ^{13}C spectrum. In practice, spectra need to be acquired at only two delay intervals, roughly corresponding to the null of the fast-relaxing component and to the full recovery of the slow component, and the subspectra are then generated by linear combination of the two. Generally, the slowly relaxing component includes less-decomposed plant residues or long-chain alkyl C, whereas fast-relaxing components may include more highly decomposed material, microbial residues, or C structures more closely associated with paramagnetics. PSRE has been applied to humin,[65] soil,[86,90] and decomposing wood,[85] and even extended to three components for dairy pond sludge.[93]

Restoration of spectra via T_{CH} and T one rho editing (RESTORE[94]) is a process that can largely correct for inefficient CP and also generates subspectra of three components: C_{SS} with short T_{CH} and $T_{1\rho H}$, C_{SL} with short T_{CH} and long $T_{1\rho H}$, and C_{LL} with long T_{CH} and $T_{1\rho H}$. C_{SL} cross-polarizes efficiently, whereas C_{SS} is underrepresented because of its short

$T_{1\rho H}$ and slow CP. In addition to a series of VCT spectra to determine T_{CH} values, three series are run with fixed T_{CH} and variable spin lock (VSL), which isolates the $T_{1\rho H}$ decay from the CP dynamics.[84] In this process, the proton magnetization is spin-locked for a variable delay before CP. The VCT curves are then fitted to a model containing components with both short and long T_{CH}, with $T_{1\rho H}$ fixed as determined from the VSL results. Corrections from these calculations resulted in a large increase in C_{obs}, especially for samples with high charcoal content (C_{LL}). Subspectra representing the three components are then generated from linear combinations of spectra taken under specified conditions, with C_{LL} giving 'virtual fractionation' of soil charcoal. The technique is very demanding with 39 acquisitions and complex data analysis, but again, for limited numbers of samples, it provides valuable insight into distinct C pools, restoration of relative intensities comparable to those obtained by DP, and reliable T_{CH} and $T_{1\rho H}$ values.

Advanced Methods for Extracting Structural Information

Subspectra of CH, CH_2, and CH_3 + C (quaternary) carbons of a humic acid were generated by linear combination of four types of CP spectra.[95] Application of DP ^{13}C NMR has always been limited by the long recycle delays required, essentially $5 \times T_{1C}$. However, a CP/T_1-TOSS method has been used to reduce recycle delays to around $1.3 \times T_{1C}$, by measuring a correction factor for each part of the spectrum.[78] This was combined with a CSA filter to isolate aromatic C, which is particularly important to separate alkyl O–C–O around 90–120 ppm, and DD was additionally used to separate protonated and nonprotonated aromatic C.[24] The CP/T_1-TOSS correction was also used to combine DP with DD for OM samples.[96] The two-dimensional (2-D) NMR spectroscopy has been very successful for solid-state NMR, and again while not routine, further structural information on ^1H–^{13}C through-space interactions can be obtained from 2-D heteronuclear correlation (HETCOR) NMR.[97] The systematic approach to the characterization of humic acid by these techniques, especially HETCOR,[98] has also applied to OM fractions from an agricultural study.[99]

Nitrogen-15 NMR

Applications of ^{15}N NMR to OM in the solid state have been limited by its combination of low natural abundance and low sensitivity (Table 1). Chemical shifts are usually referenced to nitromethane at 0 ppm, which results in negative δ values for most of the spectrum, but some studies reference anhydrous liquid ammonia at −380.23 ppm.[100] The chemistry of organic N is complex, and the potential chemical shift range very large (Table 3[6,7,101]). In general, however, studies of plant decomposition and OM,[7,10,101–106] often with ^{15}N enrichment, result in rather similar-looking spectra dominated by the broad peak of amide N from peptides, small signals of amino groups of terminal amino acids at −347 ppm, and occasional sharper signals because of nitrate and ammonium ions. Heterocyclic N may appear as a broad shoulder of the amide peak (approximately, −145 to −230 ppm). However,

Table 3. Main assignments for solid-state ^{15}N spectra referenced to nitromethane at 0 ppm[6,7,101]

Chemical shift range (ppm)	Assignment
25 to −25	Nitrate, nitrite, and nitro groups
−25 to −90	Imine, phenazines, pyridines, and Schiff bases
−90 to −145	Purine (N-7) and nitrile groups
−145 to −220	Heterocyclic N (chlorophyll, purines/pyrimidines, imidazoles, *N*-substituted pyrroles, and Maillard products)
−220 to −285	Amides/peptides, *N*-acetyl derivatives of amino sugars, tryptophanes, prolines, unsubstituted pyrroles, indoles, and carbazoles
−285 to −325	NH in guanidines, NH_2- and NR_2-groups (N_δ, N_ε-arginine, urea, nucleic acids, and aniline derivatives)
−325 to −350	Free amino groups in amino sugars and sugars
−350 to −375	NH_4^+

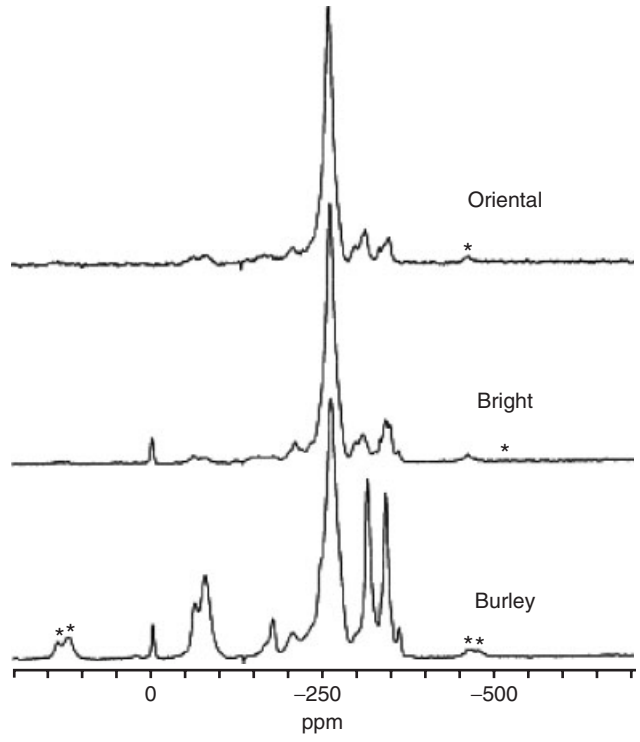

Figure 5. Solid-state ^{15}N CPMAS spectra of three varieties of tobacco leaves, referenced to nitromethane at 0 ppm (contact time = 5 ms, * = spinning side band). The lower spectrum is a variety high in nicotine (pyridine-type N at −62 and −77 ppm and pyrrolidine N at −338 ppm). (Reprinted with permission from Ref. 107. © American Chemical Society, 2004)

some plants such as tobacco have naturally high levels of heterocyclic and pyridinic N (in nicotine), resulting in a more diverse spectrum[107] (Figure 5). With increased biodegradation, pyrolysis, or geological processing, there is an increase in the proportions of heterocyclic and eventually aromatic (pyridinic) N.[25,105,108–110] Much effort has been expended to optimize acquisition parameters, especially in the search for possibly

undetected heterocyclic and aromatic N in soil.[7,106,107,111,112] In particular, CP for nonprotonated aromatic N is limited by very long T_{CH}, and acid treatment of a kerogen to protonate pyridinic N improved its detectability.[109]

However, some innovative approaches have been demonstrated. In double CP NMR,[113] intensity is first transferred from ^{1}H to the ^{15}N spin system, and then to ^{13}C where it is detected, so that the spectrum only shows ^{13}C in very close proximity to ^{15}N. It was applied to study the decomposition of doubly enriched plant residues, with the results supporting the assignment of the main ^{15}N intensity to peptides.[114] Increasing aniline N (N bonded to aromatic C) with continuous lowland rice cropping may contribute to declining N availability but is difficult to detect in OM; however, anilides were detected in a humic fraction using an indirect method based on their dipolar coupling to the naturally abundant ^{14}N nucleus.[115] Labeled substrates can be used to investigate the fate of contaminants such as 2,4,6-trinitrotoluene (TNT).[116]

Regarding detectability of pyridinic N, there do not appear to be any studies of such compounds mixed with OM, or even of behavior of sorbed ^{15}N-pyridine as done with coal[117] and clay.[118] As caffeine, nicotine, and other alkaloids may occur at high levels in some plants, interesting studies could be done by mixing such compounds with OM, rather than studying their spin dynamics in isolation. Incubations of high-alkaloid ^{15}N-enriched plants would start with less dominance of amide N, and one might ask if the effects could be detected in soils from long-term tobacco cultivation. Some ^{15}N NMR studies would benefit from additional chemical analyses, even of extractable ammonium and nitrate.

Phosphorus-31 NMR

With spin-$\frac{1}{2}$, 100% natural abundance, and high sensitivity (Table 1), ^{31}P NMR has been widely used to characterize and quantify P structures in extracts of soils and sediments,[119] but applications to solids have been much more limited. Large CSA and interactions with paramagnetics can result in substantial peak broadening, large higher order sidebands, and complete loss of signal, even with DP acquisition,[120–126] and HF pretreatment did not produce large gains, partly because of high losses of P.[127] The challenges are increased by the small chemical-shift range for P structures typically found in OM (Table 4[119]), sensitivity of chemical shifts to structural and environmental factors, its low concentration in most samples, limited potential for CP, occasional very long ^{31}P T_1 values, and lack of opportunity for isotopic enrichment. High-speed spinning is required for optimum results (i.e., at least 10 000 Hz for a 400 MHz system with ^{31}P at 161.9 MHz), and deconvolution is widely used to interpret broad, overlapping peaks.[119,121,123,124]

Chemical shifts for ^{31}P are reported with respect to external 85% H_3PO_4 at 0 ppm. The values in Table 4 are for solution spectra of OM extracts at high pH, and reports for specific phosphorus compounds and minerals, as solids should be consulted.[119,120,124,128] However, ^{31}P NMR can still provide valuable insight into nature and availability of phosphate minerals and organic P in soils,[122,124,128] sewage sludge,[129,130]

Table 4. General ranges of chemical shifts for ^{31}P referenced to 85% H_3PO_4 at 0 ppm.[119] Values are for solutions at high pH; chemical shifts in solids are highly variable and original papers should be consulted

Chemical shift range (ppm)	Assignment
20	Phosphonate (C–P bond)
5–7	Orthophosphate
6–3	Orthophosphate monoesters, one C moiety per P
2.5 to −1	Orthophosphate diesters, two C moiety per P
−4 to −5	Pyrophosphate, terminal P group of polyphosphates
−20	Polyphosphate

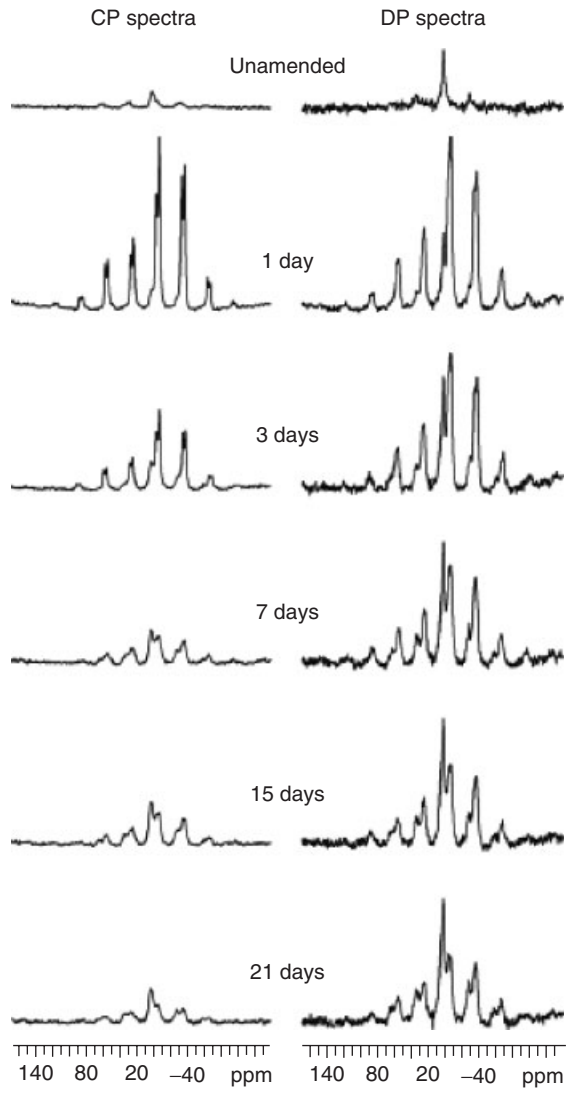

Figure 6. Solid-state ^{31}P CP and direct polarization (DP) spectra of soil before and after amendment with pyrophosphate (2000 mg P kg^{-1}). The vertical scales allow direct comparison of CP and DP intensities. Pyrophosphate occurs at −8.5 ppm, and the time series shows increasing conversion to orthophosphate at 2.1 ppm. (Reproduced with permission from Ref. 128. © Soil Science Society of America, 2006)

manure,[93] and composts.[103] Figure 6 shows the transformation of pyrophosphate to orthophosphate after addition to soil.[128] With highly organic samples low in paramagnetic metals, SSB are not always a large problem, and the increased availability of high-speed spinning should facilitate applications of ^{31}P NMR. It has also been combined with ^{27}Al NMR to investigate soil Al–P interactions[123] and used in model systems to investigate the fate of environmental contaminants.[131,132]

Biographical Sketch

Caroline Preston was born in 1948. She finished her BSc, 1970, and PhD, 1975, in Vancouver. After a PhD on proton relaxation of carbohydrates in solution and postdoc on Raman spectroscopy, she joined Agriculture Canada in 1978, moving to the Canadian Forest Service in 1986. With a succession of NMR instruments, some preowned, applied solution- and solid-state NMRs, along with stable isotope techniques and wet chemistry, to a wide range of soil, plant, and fertilizer (contributed over 120 papers and chapters). She retired in 2008 but is still writing and dabbling in NMR, tannins, and forest fires.

Related Articles

Environmental Comprehensive Multiphase NMR; Soil Organic Matter; Forest Ecology and Soils; Organic Pollutants in the Environment

References

1. R. K. Harris, E. D. Becker, S. M. C.de Menezes, R. Goodfellow, and P. Granger, *Solid State NMR*, 2002, **22**, 458.
2. D. I. Hoult, *Concepts Magn. Reson.*, 2009, **34A**, 193.
3. P. Kinchesh, D. S. Powlson, and E. W. Randall, *Eur. J. Soil Sci.*, 1995, **46**, 125.
4. K. J. Dria, J. R. Sachleben, and P. G. Hatcher, *J. Environ. Qual.*, 2002, **31**, 393.
5. V. J. Bartuska, G. E. Maciel, J. Schaefer, and E. O. Stejskal, *Fuel*, 1977, **56**, 354.
6. I. Kögel-Knabner, *Geoderma*, 1997, **80**, 243.
7. H. Knicker and H.-D. Lüdemann, *Org. Geochem.*, 1995, **23**, 329.
8. I. Kögel-Knabner, *Soil Biol. Biochem.*, 2002, **34**, 139.
9. C. M. Preston, J. A. Trofymow, and CIDET Working Group, *Can. J. Bot.*, 2000, **78**, 1269.
10. H. Knicker, *J. Environ. Qual.*, 2000, **29**, 715.
11. J. I. Hedges, G. Eglinton, P. G. Hatcher, D. L. Kirchman, C. Arnosti, S. Derenne, R. P. Evershed, I. Kögel-Knabner, J. W.de Leeuw, R. Littke, W. Michaelis, and J. Rullkötter, *Org. Geochem.*, 2000, **31**, 945.
12. J. S. Waugh, *Anal. Chem.*, 1993, **65**, 725A.
13. G. E. Maciel, *Science*, 1984, **226**, 282.
14. J. Schaefer and E. O. Stejskal, *J. Am. Chem. Soc.*, 1976, **98**, 1031.
15. P. G. Hatcher, D. L. VanderHart, and W. L. Earl, *Org. Geochem.*, 1980, **2**, 87.
16. C. M. Preston and J. A. Ripmeester, *Can. J. Spectrosc.*, 1982, **27**, 99.
17. M. A. Wilson, R. J. Pugmire, K. W. Zilm, K. M. Goh, S. Heng, and D. M. Grant, *Nature*, 1981, **294**, 648.
18. C. M. Preston, *Soil Sci.*, 1996, **161**, 144.
19. C. M. Preston, *Can. J. Soil Sci.*, 2001, **81**, 255.
20. D. L. Bryce, G. M. Bernard, M. Gee, M. D. Lumsden, K. Eichele, and R. E. Wasylishen, *Can. J. Anal. Sci. Spectrosc.*, 2001, **46**, 46.
21. A. E. Bennett, C. M. Rienstra, M. Auger, K. V. Lakshmi, and R. G. Griffin, *J. Chem. Phys.*, 1995, **103**, 6951.
22. E. R. Andrew, A. Bradbury, and R. G. Eades, *Nature*, 1959, **183**, 1802.
23. I. J. Lowe, *Phys. Rev. Lett.*, 1959, **2**, 285.
24. J.-D. Mao and K. Schmidt-Rohr, *Environ. Sci. Technol.*, 2004, **38**, 2680.
25. H. Knicker, *Org. Geochem.*, 2011, **42**, 867.
26. C. M. Preston, C. H. Shaw, J. S. Bhatti, and R. M. Siltanen, in Soil C and N Pools in Forested Upland and Non-forested Lowland Sites Along the Boreal Forest Transect Case Study in Central Canada, eds C. H. Shaw and M. J. Apps, Natural Resources Canada: Edmonton, AB, 2002, 155.
27. A. Pines, M. G. Gibby, and J. S. Waugh, *J. Chem. Phys.*, 1973, **59**, 569.
28. S. R. Hartmann and E. L. Hahn, *Phys. Rev.*, 1962, **128**, 2042.
29. L. B. Alemany, D. M. Grant, R. J. Pugmire, T. D. Alger, and K. W. Zilm, *J. Am. Chem. Soc.*, 1983, **105**, 2133.
30. W. Kolodziejski and J. Klinowski, *Chem. Rev.*, 2002, **102**, 613.
31. L. B. Alemany, D. M. Grant, R. J. Pugmire, T. D. Alger, and K. W. Zilm, *J. Am. Chem. Soc.*, 1983, **105**, 2142.
32. L. B. Alemany, D. M. Grant, T. D. Alger, and R. J. Pugmire, *J. Am. Chem. Soc.*, 1983, **105**, 6697.
33. C. M. Preston, J. R. Nault, and J. A. Trofymow, *Ecosystems*, 2009, **12**, 1078.
34. R. J. Smernik and J. M. Oades, *Geoderma*, 2000, **96**, 101.
35. G. Metz, X. Wu, and S. O. Smith, *J. Magn. Reson. Ser. A*, 1994, **110**, 219.
36. R. L. Cook, C. H. Landford, R. Yamdagni, and C. M. Preston, *Anal. Chem.*, 1996, **68**, 3979.
37. A. E. Berns and P. Conte, *Org. Geochem.*, 2011, **42**, 926.
38. W. T. Dixon, J. Schaefer, M. D. Sefcik, E. O. Skejskal, and R. A. McKay, *J. Magn. Reson.*, 1982, **80**, 341.
39. D. E. Axelson, Solid State Nuclear Magnetic Resonance of Fossil Fuels: An Experimental Approach, Ministry of Supply and Services Canada: Ottawa, 1985, 226.
40. J. Hirschinger, *Solid State NMR*, 2008, **34**, 210.
41. D. E. Axelson, *Fuel*, 1987, **66**, 195.
42. S. A. Quideau, M. A. Anderson, R. C. Graham, O. A. Chadwick, and S. E. Trumbore, *For. Ecol. Manage.*, 2000, **138**, 19.
43. S. J. Opella and M. H. Frey, *J. Am. Chem. Soc.*, 1979, **101**, 5854.
44. W. L. Earl and D. L. Vanderhart, *Macromolecules*, 1979, **12**, 762.
45. W.-G. Hu, J. Mao, B. Xing, and K. Schmidt-Rohr, *Environ. Sci. Technol.*, 2000, **34**, 530.
46. I. Kögel-Knabner and P. G. Hatcher, *Sci. Total Environ.*, 1989, **81/82**, 169.
47. P. G. Hatcher, *Org. Geochem.*, 1987, **11**, 31.
48. R. H. Newman, *J. Magn. Reson.*, 1990, **86**, 176.
49. C. M. Preston, P. Sollins, and B. G. Sayer, *Can. J. For. Res.*, 1990, **20**, 1382.
50. M. A. Wilson, R. J. Pugmire, and D. M. Grant, *Org. Geochem.*, 1983, **5**, 121.
51. R. H. Newman, *J. Magn. Reson.*, 1992, **96**, 370.
52. R. J. Smernik and J. M. Oades, *Eur. J. Soil. Sci.*, 2001, **52**, 103.
53. P. G. Hatcher and M. A. Wilson, *Org. Geochem.*, 1991, **17**, 293.
54. R. J. Smernik, *Eur. J. Soil. Sci.*, 2006, **57**, 665.
55. F. Ziarelli and S. Caldarelli, *Solid State NMR*, 2006, **29**, 214.
56. R. J. Smernik and J. M. Oades, *Geoderma*, 1999, **89**, 219.

57. R. J. Smernik and J. M. Oades, *Geoderma*, 2000, **96**, 151.
58. I. Schöning, H. Knicker, and I. Kögel-Knabner, *Org. Geochem.*, 2005, **36**, 1378.
59. J.-M. Séquaris, H. Philipp, H.-D. Narres, and H. Vereecken, *Eur. J. Soil Sci.*, 2008, **59**, 592.
60. C. M. Preston, M. Schnitzer, and J. A. Ripmeester, *Soil Sci. Soc. Am. J.*, 1989, **53**, 1442.
61. M. W. I. Schmidt, H. Knicker, P. G. Hatcher, and I. Kögel-Knabner, *Eur. J. Soil Sci.*, 1997, **48**, 319.
62. M. J. Simpson and P. G. Hatcher, *Org. Geochem.*, 2004, **35**, 923.
63. M. J. Simpson and C. Preston, in Soil Sampling and Methods of Analysis, 2nd edn, eds M. R. Carter and E. G. Gregorich, CRC Press: Boca Raton, FL, 2008, Chapter 53.
64. C. Rumpel, N. Rabia, S. Derenne, K. Quenea, K. Esterhues, I. Kögel-Knabner, and A. Mariotti, *Org. Geochem.*, 2006, **37**, 1437.
65. C. M. Preston and R. H. Newman, *Geoderma*, 1995, **68**, 229.
66. M. W. I. Schmidt and G. Gleixner, *Eur. J. Soil Sci.*, 2005, **56**, 407.
67. K. H. Dai and C. E. Johnson, *Geoderma*, 1999, **93**, 289.
68. C. N. Gonçalves, R. S. D. Dalmolin, D. P. Dick, H. Knicker, E. Klamt, and I. Kögel-Knabner, *Geoderma*, 2003, **116**, 373.
69. C. M. Preston, R. L. Dudley, C. A. Fyfe, and S. P. Mathur, *Geoderma*, 1984, **33**, 245.
70. M. Schilling and W. T. Cooper, *Environ. Sci. Technol.*, 2004, **38**, 5059.
71. E. H. Novotny, H. Knicker, L. A. Colnago, and L. Martin-Neto, *Org. Geochem.*, 2006, **37**, 1562.
72. C. Keeler and G. E. Maciel, *Anal. Chem.*, 2003, **75**, 2421.
73. X. Fang, T. Chua, K. Schmidt-Rohr, and M. L. Thompson, *Geochim. Cosmochim. Acta*, 2010, **74**, 584.
74. K. Esterhues, C. Rumpel, and I. Kögel-Knabner, *Org. Geochem.*, 2007, **38**, 1356.
75. R. J. Smernik and J. M. Oades, *Solid State NMR*, 2001, **20**, 74.
76. Q. Chen, S. S. Hou, and K. Schmidt-Rohr, *Solid State NMR*, 2004, **26**, 11.
77. M. F. Davis, H. R. Schroeder, and G. E. Maciel, *Holzforschung*, 1994, **48**, 99.
78. J.-D. Mao, W.-G. Hu, K. Schmidt-Rohr, G. Davies, E. A. Ghabbour, and B. Xing, *Soil Sci. Soc. Am. J.*, 2000, **64**, 873.
79. J. A. Baldock, C. A. Masiello, Y. Gélinas, and J. I. Hedges, *Mar. Chem.*, 2004, **92**, 39.
80. L. Cécillon, G. Certini, H. Lange, C. Forte, and L. T. Strand, *Org. Geochem.*, 2012, **46**, 127.
81. J. Kaal, J. A. Baldock, P. Buurman, K. G. J. Nierop, X. Pontevedra-Pombal, and A. Martínez-Cortizas, *Org. Geochem.*, 2007, **38**, 1097.
82. M. J. Simpson and J. R. McKelvie, *Anal. Bioanal. Chem.*, 2009, **394**, 137.
83. B. Nordén and C. Albano, *Fuel*, 1989, **68**, 771.
84. K. Abelmann, K. U. Totsche, H. Knicker, and I. Kögel-Knabner, *Solid State NMR*, 2004, **25**, 252.
85. C. M. Preston, R. J. Smernik, R. F. Powers, J. G. McColl, and T. M. McBeath, *Org. Geochem.*, 2011, **42**, 936.
86. C. M. Preston, R. H. Newman, and P. Rother, *Soil Sci.*, 1994, **157**, 26.
87. M. A. Wilson, A. M. Vassallo, E. M. Perdue, and J. H. Reuter, *Anal. Chem.*, 1987, **59**, 551.
88. A. E. Berns and P. Conte, *Open Magn. Reson. J.*, 2010, **3**, 75.
89. I. Bergman, P. Lundberg, C. M. Preston, and M. Nilsson, *Soil Sci. Soc. Am. J.*, 2000, **64**, 1368.
90. R. J. Smernik, *Geoderma*, 2005, **125**, 249.
91. J. A. Baldock, J. M. Oades, A. M. Vassallo, and M. A. Wilson, *Aust. J. Soil Res.*, 1990, **28**, 213.
92. R. H. Newman and K. R. Tate, *J. Soil Sci.*, 1991, **42**, 39.
93. R. H. Newman and L. M. Condron, *Solid State NMR*, 1995, **4**, 259.
94. R. J. Smernik and J. M. Oades, *Eur. J. Soil Sci.*, 2003, **54**, 103.
95. C. Keeler and G. E. Maciel, *J. Mol. Struct.*, 2000, **550–551**, 297.
96. G. Ding and J. A. Rice, *Geoderma*, 2012, **189–190**, 381.
97. J.-D. Mao, B. Xing, and K. Schmidt-Rohr, *Environ. Sci. Technol.*, 2001, **35**, 1928.
98. J.-D. Mao, N. Chen, and X. Cao, *Org. Geochem.*, 2011, **42**, 891.
99. X. Cao, D. C. Olk, M. Chappell, C. A. Cambardella, L. F. Miller, and J. Mao, *Soil Sci. Soc. Am. J.*, 2011, **75**, 1374.
100. P.-H. Hsu and P. G. Hatcher, *Org. Geochem.*, 2006, **37**, 1694.
101. N. Maie, H. Knicker, A. Watanabe, and M. Kimura, *Org. Geochem.*, 2006, **37**, 12.
102. L. Benzing-Purdie, J. A. Ripmeester, and C. M. Preston, *J. Agric. Food Chem.*, 1983, **31**, 913.
103. C. M. Preston, J. A. Ripmeester, S. P. Mathur, and M. Lévesque, *Can. J. Spectrosc.*, 1986, **31**, 63.
104. P. W. Clinton, R. H. Newman, and R. B. Allen, *Eur. J. Soil Sci.*, 1995, **46**, 551.
105. H. Knicker, P. G. Hatcher, and F. J. González-Vila, *J. Environ. Qual.*, 2002, **31**, 444.
106. R. J. DiCosty, D. P. Weliky, S. J. Anderson, and E. A. Paul, *Org. Geochem.*, 2003, **34**, 1635.
107. Z. Ma, D. H. Barich, M. S. Solum, and R. J. Pugmire, *J. Agric. Food Chem.*, 2004, **52**, 215.
108. H. Knicker, G. Almendros, F. J. González-Vila, F. Martin, and H.-D. Lüdemann, *Soil Biol. Biochem.*, 1996, **28**, 1053.
109. S. R. Kelemen, M. Afeworki, M. L. Gorbaty, P. J. Kwiatek, M. S. Solum, J. Z. Hu, and R. J. Pugmire, *Energy Fuels*, 2002, **16**, 1507.
110. S. R. Kelemen, M. Afeworki, M. L. Gorbaty, P. J. Kwiatek, M. Sansone, C. C. Walters, and A. D. Cohen, *Energy Fuels*, 2006, **20**, 635.
111. R. J. Smernik and J. A. Baldock, *Biogeochemistry*, 2005, **75**, 507.
112. R. J. Smernik and J. A. Baldock, *Plant Soil*, 2005, **275**, 271.
113. J. Schaefer, E. O. Stejskal, J. R. Garbow, and R. A. McKay, *J. Magn. Reson.*, 1984, **59**, 150.
114. H. Knicker, *Org. Geochem.*, 2002, **33**, 237.
115. K. Schmidt-Rohr, J.-D. Mao, and D. C. Olk, *Proc. Natl. Acad. Sci. U. S. A.*, 2004, **101**, 6351.
116. H. Knicker, C. Achtnich, and H. Lenke, *J. Environ. Qual.*, 2001, **30**, 403.
117. J. A. Ripmeester, R. E. Hawkins, J. A. MacPhee, and B. N. Nandi, *Fuel*, 1986, **65**, 740.
118. L. Ukrainczyk and K. A. Smith, *Environ. Sci. Technol.*, 1996, **30**, 3167.
119. B. J. Cade-Menun, *Talanta*, 2005, **66**, 359.
120. Z. He, C. W. Honeycutt, T. Zhang, P. J. Pellechia, and W. A. Caliebe, *Soil Sci. Soc. Am. J.*, 2007, **71**, 940.
121. P. Conte, D. Šmejkalová, A. Piccolo, and R. Spaccini, *Eur. J. Soil Sci.*, 2008, **59**, 584.
122. W. J. Dougherty, R. J. Smernik, and D. J. Chittleborough, *Soil Sci. Soc. Am. J.*, 2005, **69**, 2058.
123. R. Lookman, P. Grobet, R. Merckx, and W. H. Van Riemsdijk, *Geoderma*, 1997, **80**, 369.
124. R. W. McDowell, L. M. Condron, N. Mahieu, P. C. Brookes, P. R. Poulton, and A. N. Sharpley, *J. Environ. Qual.*, 2002, **31**, 450.

125. C. A. Shand, M. V. Cheshire, C. N. Bedrock, P. J. Chapman, A. R. Fraser, and J. A. Chudek, *Plant Soil*, 1999, **214**, 153.
126. B. Sutter, R. E. Taylor, L. R. Hossner, and D. W. Ming, *Soil Sci. Soc. Am. J.*, 2002, **66**, 455.
127. W. J. Dougherty, R. J. Smernik, E. K. Bünemann, and D. J. Chittleborough, *Soil Sci. Soc. Am. J.*, 2007, **71**, 1111.
128. T. M. McBeath, R. J. Smernik, E. Lombi, and M. J. McLaughlin, *Soil Sci. Soc. Am. J.*, 2006, **70**, 856.
129. Z. R. Hinedi, A. C. Chang, and J. P. Yesinowski, *Soil Sci. Soc. Am. J.*, 1989, **53**, 1053.
130. Z. R. Hinedi and A. C. Chang, *Soil Sci. Soc. Am. J.*, 1989, **53**, 1057.
131. D. M. Mizrahi and I. Columbus, *Environ. Sci. Technol.*, 2005, **39**, 8931.
132. J. A. Shaw, R. K. Harris, and P. R. Norman, *Langmuir*, 1998, **14**, 6716.

Further Reading

1. A. J. Simpson, D. J. McNally, and M. J. Simpson, *Prog. NMR Spectrosc.*, 2011, **58**, 97.
2. J. Schaefer, E. O. Stejskal, and R. Buchdahl, *Macromolecules*, 1977, **10**, 384.
3. D. L. VanderHart, W. L. Earl, and A. N. Garroway, *J. Magn. Reson.*, 1981, **44**, 361.
4. D. L. VanderHart and G. C. Campbell, *J. Magn. Reson.*, 1998, **134**, 88.
5. M. A. Wilson, NMR Techniques and Applications in Geochemistry and Soil Chemistry, Pergamon Press: Oxford, 1987.